The orbit, atmospheric dynamics, and initial mass of the Park Forest meteorite

P. BROWN,[1]* D. PACK,[2] W. N. EDWARDS,[3] D. O. ReVELLE,[4] B. B. YOO,[5]
R. E. SPALDING,[6] and E. TAGLIAFERRI[7]

[1]Canada Research Chair in Meteor Science, Department of Physics and Astronomy, University of Western Ontario,
London, Ontario, N6A 3K7, Canada
[2]Space Science Applications Laboratory, Laboratory Operations, Aerospace Corporation, 2350 East El Segundo Boulevard, El Segundo,
California 90245–4691, USA
[3]Department of Earth Sciences, University of Western Ontario, London, Ontario, N6A 5B7, Canada
[4]Atmospheric, Climate and Environmental Dynamics, Meteorological Modeling Team, P.O. Box 1663, MS D401,
Los Alamos National Laboratory, Los Alamos, New Mexico 87545, USA
[5]Astrodynamics Department, Systems Engineering Division, Aerospace Corporation, 2350 East El Segundo Boulevard,
El Segundo, California 90245–4691, USA
[6]Sandia National Laboratory, Org. 5740, MS 0973, P.O. Box 5800, Albuquerque, New Mexico 87185, USA
[7]Space-Based Surveillance Division, Aerospace Corporation, 2350 East El Segundo Boulevard, El Segundo, California 90245–4691, USA
*Corresponding author. E-mail: pbrown@uwo.ca

Abstract–The fireball accompanying the Park Forest meteorite fall (L5) was recorded by ground-based videographers, satellite systems, infrasound, seismic, and acoustic instruments. This meteorite shower produced at least 18 kg of recovered fragments on the ground (Simon et al. 2004). By combining the satellite trajectory solution with precise ground-based video recording from a single site, we have measured the original entry velocity for the meteoroid to be 19.5 ± 0.3 km/s. The earliest video recording of the fireball was made near the altitude of 82 km. The slope of the trajectory was 29° from the vertical, with a radiant azimuth (astronomical) of 21° and a terminal height measured by infrared satellite systems of 18 km. The meteoroid's orbit has a relatively large semi-major axis of 2.53 ± 0.19 AU, large aphelion of 4.26 ± 0.38 AU, and low inclination. The fireball reached a peak absolute visual magnitude of −22, with three major framentation episodes at the altitudes of 37, 29, and 22 km. Acoustic recordings of the fireball airwave suggest that fragmentation was a dominant process in production of sound and that some major fragments from the fireball remained supersonic to heights as low as ~10 km. Seismic and acoustic recordings show evidence of fragmentation at 42, 36, 29, and 17 km. Examination of implied energies/initial masses from all techniques (satellite optical, infrasound, seismic, modeling) leads us to conclude that the most probable initial mass was $(11 \pm 3) \times 10^3$ kg, corresponding to an original energy of ~0.5 kt TNT (2.1×10^{12} J) and a diameter of 1.8 m. These values correspond to an integral bolometric efficiency of $7 \pm 2\%$. Early fragmentation ram pressures of <1 MPa and major fragmentations occurring with ram pressures of 2–5 MPa suggest that meter-class stony near-Earth asteroids (NEAs) have tensile strengths more than an order of magnitude lower than have been measured for ordinary chondrites. One implication of this observation is that the rotation period for small, fast-rotating NEAs is likely to be >30 seconds.

INTRODUCTION

The fall of the Park Forest meteorite (classified by Simon et al. [2004] as an L5 chondrite) occurred on March 27, 2003 UT (March 26, 2003 local date) at 05:50 UT (11:50 PM local time) in the southern suburbs of Chicago. Many local residents noted the bright fireball accompanying the meteorite

fall as well as intense sonic detonations shortly after the visible part of the fireball ceased. Park Forest is unique in being the first major meteorite fall to occur in modern times in an urban area; this fact has led to the recovery of many fragments of the fall as described in Simon et al. (2004). Park Forest is also unusual in its size/initial energy—an object with the energy of Park Forest collides with Earth about half a

dozen times per annum (Brown et al. 2002a), with only about two events of comparable or greater energy expected over land in any given year.

Fireball data provide one important observational element to the understanding of the evolution of material from source regions in the main asteroid belt (Morbidelli and Gladman 1998) and a means to gauge the flux of small bodies to Earth (Brown et al. 2002a). Detailed data from different sensors also allow calibration of fireball data, notably luminous efficiencies and masses of impacting bodies. The wealth of ancillary information (and ground-truth in the form of meteorites) connected with the Park Forest fireball makes its study of particular interest. These data have allowed constraints to be placed on the dynamics, breakup behavior, and orbit of the Park Forest fireball, both to provide context for the recovered meteorite samples and as part of our broader program of large fireball study (cf. Brown et al. 1996; Brown et al. 2002b; ReVelle et al. 2004). The goal of this program is to document the entry of large meteoroids (or small asteroids) into Earth's atmosphere using as many different instrumental techniques as possible as a method to measure the physical structure of the original bodies and as a means to constrain the process of ablation. Such constraints are necessary observational inputs to models of large meteoroid ablation which aim to determine the large meteorite flux at Earth and/ or estimate ground damage from bolide airbursts (cf. Bland and Artmemeva 2003; ReVelle and Ceplecha 2002; Hills and Goda 1993).

Here we analyze the U.S. Department of Energy (DoE) and the Department of Defense (DoD) satellite data for the 27 March, 2003 Park Forest bolide. The meteoroid's energy, trajectory, and velocity—and thus the mass and size of the object—are derived from the satellite data coupled with entry modeling of the event. Seven previous fireballs producing meteorite falls provided sufficient data for the estimation of meteoroid velocities, trajectories, and orbits prior to Earth impact; Park Forest marks the eighth meteorite fall with an accurately measured pre-atmospheric orbit. All these bodies were in orbits consistent with Apollo-type Earth-crossing asteroids (cf. Borovička et al. 2003; Spurny et al. 2003). Additional data from ground-based video cameras are fused with the satellite data to refine the determination of velocity. In addition to the satellite data, the Park Forest bolide was measured with ground-based instruments including infrasonic, seismic, and acoustic microphones. These additional data sources provide estimates of the energy release and the pre-atmospheric mass of the object.

VIDEO DATA

In total, at least seven videos of the Park Forest fireball were recorded from the Chicago area. Of these, five showed only local brightening of the landscape in response to the brightest portion of the fireball. The two direct videos of the fireball were shot by video in police cruisers; one captured only the terminal portion of the flight while the car was moving and is of limited use for astrometric purposes. The other video was captured by Sgt. Kyle Griffith of the South Haven Police Department (42.4093°N 86.2598°W, altitude 210 m) from a permanently mounted camera in a stationary car and records the very earliest portions of the fireball flight (Fig. 1). The terminal portions of the flight (including two of the three major flares) are obstructed by trees in the foreground of the image. To calibrate this video, theodolite measurements of foreground objects were made from the location of the original video recording. In addition, nighttime stellar calibrations of the same field were made. These stellar calibrations were then digitally mapped to the original video field and the resulting azimuths of foreground fiducial objects were compared to the theodolite measurements following the general technique described by Borovička et al. (2003). An average systematic difference of +0.9° in azimuth and +0.4° in elevation noted between the two sets of measurements can be attributed to a probable offset in the theodolite reference. When this systematic bias is removed, the average standard deviation of the remaining measurements is 0.3°—taken to be representative of the random internal error between the absolute values for individual measurements. Much of this error is perpendicular to the fireball track, with the relative error along the track smaller by a factor of three and corresponding to a mean deviation of ~1 km perpendicular to the trajectory at the average range of the fireball from South Haven, Michigan (200 km) and less than 300 m along the fireball track (between video frames).

In connection with measurement error, we emphasize that many of the fiducial points closest to the apparent fireball path were portions of trees and that these had noticeably changed at the time of the July calibrations relative to the March police video. Similarly, the brightest portions of the video fireball record suffer from extreme blooming of the image, though we have attempted to use the centroid of the bloomed image in each frame. Thus, we expect the relative difference between the video sightlines to have approximately the precision noted above, but a systematic error may still be present due to the changes in the fiducial points between the time of the fireball in March and the measurements in July.

Examination of these video data establishes that three major and possibly as many as three minor flares occurred during the fireball's flight. To estimate the temporal spacing of the flares, the total pixel intensity in each frame for each video was summed; the scaled result of this procedure is shown in Fig. 2. Clearly, for several videos, the automatic gain control plays a major role in suppressing the later/ brighter portions of the fireball where blooming is severe. However, the relative spacing of the brightness maxima is identical to within a single frame on all videos.

In addition to these optical data, a single security camera

Fig. 1. A composite of several frames of the video taken at South Haven, Michigan of the Park Forest fireball. Only the earliest frames (prior to major fragmentation events) are shown for clarity.

in Momence, Illinois recorded the audible detonations associated with the fireball approximately 2.5 minutes after the optical registration of the event. More detailed discussion of this signal and the seismic data will follow.

SATELLITE LIGHT CURVE DATA

Visible light satellite sensors operated by the U.S. DoE for nuclear monitoring purposes routinely record high-energy meteor events such as the Park Forest bolide (Tagliaferri et al. 1994). Useful information about meteor flaring and breakup is contained in the intensity versus time data from these sensors. From these data, the total radiated energy was 1.42×10^{11} J and the peak intensity 4.2×10^{10} Watts/steradian. These optical intensity and energy results assume the emitting source to be a 6000 K black body as in past work (McCord et al. 1995; Brown et al. 1996). Deviations in temperature of ~1500 K from our 6000 K assumption produce variations in these numbers of a few tens of percent. Using the conversion factors described in Ceplecha et al. (1998) for a 6000 K black body, a value of 4.2×10^{10} Watts/steradian corresponds to an equivalent peak absolute visual magnitude for Park Forest of −21.7. Three distinct intensity features are readily apparent in the satellite light curve. There is excellent correlation of the three main temporal features between the space sensor and ground-based video data, with the peaks matching to within ±1 video frame (±1/30th of a second) as shown in Fig. 3. Note that the video light curve intensities are affected by the autogain mechanism. The initial kinetic energy of the meteoroid may be estimated using the empirical scaling factor from Brown et al. (2002a). It ties satellite optical energy to ground-truthed energy values found by using independent

energy estimates for those satellite events which were meteorite falling events or infrasonic signal measurements of the energy release. For the 1.42×10^{11} J optical energy value and using the scaling formula for the bolometric luminous efficiency τ of Brown et al. (2002a) of:

$$\tau = (0.1212 \pm 0.0043)E_o^{0.115 \pm 0.075} \qquad (1)$$

where E_o is the optical measured energy under the assumption of a 6000 K black body and the total initial kinetic energy is simply given by E_o/τ. We find an energy to optical energy conversion efficiency from this relation of 8.2% ± 2% implying an initial kinetic energy of 0.41 ± 0.09 kt TNT equivalent or $(1.7 \pm 0.4) \times 10^{12}$ J.

Satellite Trajectory Data and Velocity Estimation

An accurate trajectory for the meteor has been generated from the U.S. DoD IR sensor measurements. The U.S. DoD IR sensors scanned the emissive track from the passage of the meteor through the atmosphere. The first IR measurement was timed 0.60 sec following the main peak of the visible light curve. This is about 0.03 sec after the final flare feature, so the timing was excellent for measuring the emission left from the passage of the object through the atmosphere. The second IR measurement was taken 0.84 sec following the peak optical signal, the derived flight path angle being 29° from the local geocentric vertical and the flight path azimuth 21°—the object traveled from the SSW to the NNE). The straight-line intersection of the track with the WGS-84 ellipsoid (NIMA 2000) is at a geodetic latitude of 41.55°N and a longitude of 87.68°W. The IR satellite emissive track was approximately 23 km long and extended from 39 km to
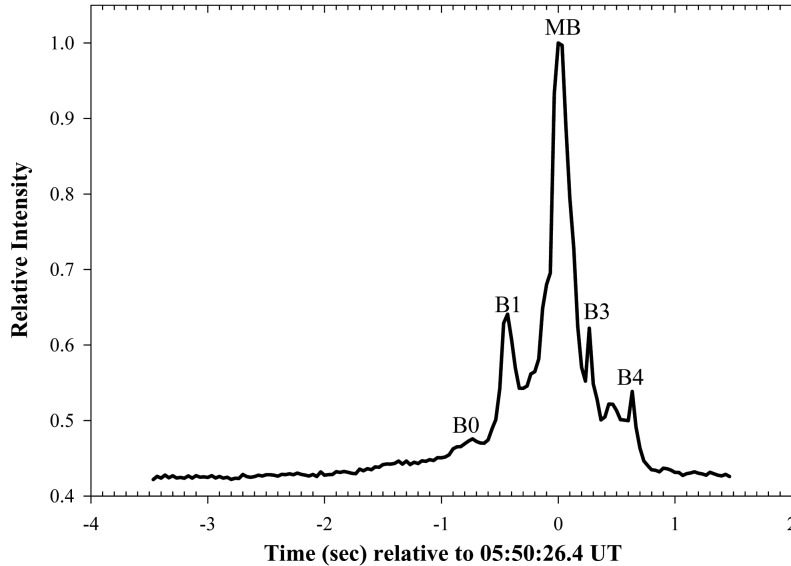
Fig. 2. Photometry of the fireball from the South Haven, Michigan video. The total value for all pixels are summed in each image and normalized to the value at the peak (corresponding to the time of the major fragmentation). Note the ordinate is in linear units (not logarithmic as would be the case for stellar magnitudes) to accentuate the smaller features in the light curve.

Table 1. Velocities calculated from features in visible and infrared space sensor data.

Altitude range (km)	Velocity (km/s)
37–29	20 ± 1
37–22	17 ± 1
29–22	14 ± 1

18 km altitude above the Earth's surface. We did not use the video measured sightlines in the trajectory solution due to concern with the absolute accuracy of the measurements as a result of the uncertain fiducial points close to the fireball path as described earlier.

Three distinct intensity peaks were evident along the track at the altitudes of 37 km, 29 km, and 22 km. Correlating these with the three temporal features evident in the light curves (both satellite and video) allows velocity to be estimated over intervals along the track. The bright flares are aligned between the video sightlines and satellite trajectory by systematically increasing the video sightline azimuths by 1.0 degree and the altitudes by 1.98 degrees. Here, the assumption is made that the flares observed in the satellite optical light curve correspond to the bright features along the IR emissive track. With such a correlation, the average velocity of the object between intensity features calculated based on the satellite astrometry alone is shown in Table 1. The satellite-only velocity and deceleration measured are physically reasonable based on past observations and modeling. A self-consistent check on the results above estimates the average meteoroid velocity along its entire track from the total length of the emissive streak divided by the

duration of the meteor light curve signal. The accuracy of this method depends on the fortuitous timing of the infrared scanning of the meteor track. Applying this approach yields 19 km/s, in fair agreement with the 17 km/s result from the 37–22 km center segment of the track. From the high-altitude results in Table 1, the best estimate of the initial velocity of the meteoroid using satellite data alone is ~20 km/s. The object decelerated to ~14 km/s at lower altitudes.

This initial velocity (20 km/s), coupled with our energy computed from the satellite optical light curve yield an equivalent pre-atmospheric mass of $(8.6 \pm 1.9) \times 10^3$ kg. A further refinement of the initial velocity is possible by making use of the trajectory defined by the satellite observations and using the sightlines from the Southhaven fireball video together. In particular, we projected the sightlines from every third video frame (separated by 0.1 sec in time) onto the satellite trajectory plane of the fireball to provide a more robust velocity estimation in the early portion of the path. The video and satellite data were combined using the B1 burst (Fig. 3) clearly observed in the Southhaven video (and measurable as the fireball had not been obscured by trees at this point) and the satellite IR data as a fiducial point. The velocity profile produced shows no measurable deceleration above 60 km altitude, as would be expected for a body as large as Park Forest (Ceplecha et al. 1998). The average velocity from first detection (82 km altitude) to the 60 km level produces a mean velocity of 19.5 ± 0.3 km/s. This value is found by simply taking the total along-track distance measured in the video between these heights and dividing by the total elapsed time. We take this to be the best estimate for the initial entry velocity for the Park Forest meteoroid.
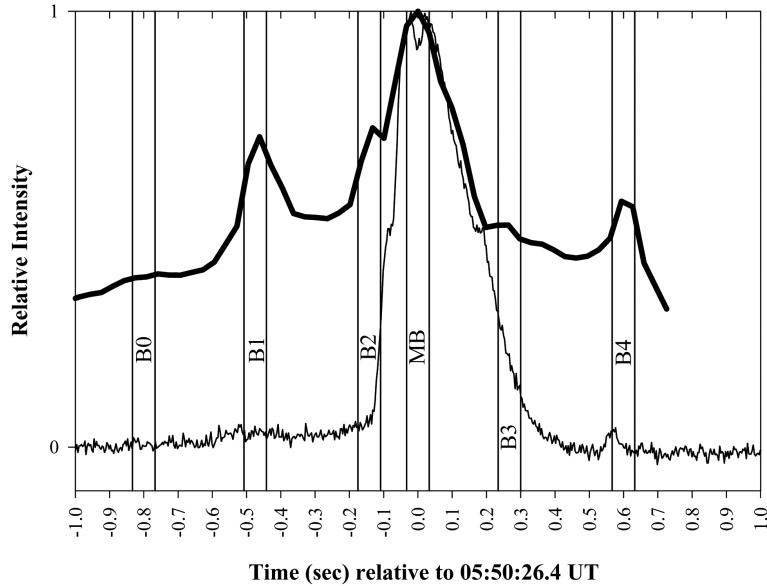
Fig. 3. Comparison of space-based and ground-based light curves of the Park Forest fireball. The solid curve is a measure of the normalized frame-by-frame integrated pixel intensity values for one of the indirect videos showing most of the major features visible across the entire set of videos. The thin line is the normalized light curve from the U.S. DoE sensor data. Some of the features visible in the video data (notably B2 and B3) may be artifacts of the auto-gain control of the video systems. The time in seconds is relative to March 27, 2003 05:50:26.4 UT.

Table 1a shows the measured average velocity across the consecutive sets of nine video frames. As the random along-track error is on the order of 0.1 degrees, close to ~5% of the average angular separation between subsequent points separated by only nine-frames, there is necessarily a large amount of error (and wander) for each measured point shown in the table.

ORBIT AND TRAJECTORY

The mean velocity found in the previous section is within the error margins of the satellite-only velocity solution for the earliest portion of the trajectory (cf. Table 1); since the time bases for both are independent, this is a reassuring cross-check. We adopt the azimuth and zenith angles of the apparent radiant derived from the satellite data. These measurements produce final values of $Z = 29°$ and $A = 21°$. Taking this radiant and $V_\infty = 19.5 \pm 0.3$ km/s produces the trajectory given in Table 2 and orbit (following the procedure given in Ceplecha 1987) in Table 3 and in Fig. 4. We note that this orbit is a typical orbit of an Apollo asteroid and is comparable to the other seven meteorites, the orbits of which are known (Borovička et al. 2003). The orbit for Park Forest is known with a precision ~10 times less than the five best measured fireball-meteorite pairs (Pribram, Innisfree, Lost City, Peekskill, and Neuschwanstein) and with comparable precision to the recent Morávka fall (but more precisely than the Tagish Lake carbonaceous chondrite) (cf. Borovička et al. 2003; Spurny et al. 2003; Brown et al. 2000).

Employing the model of Bottke et al. (2001) which uses a, e, i combinations and a source model for NEAs in the main

Table 1a. Velocity measurements and errors based on average motion across nine video frames for the upper portion of the trajectory. Heights represent the mid-point of the nine-frame average. The error is computed from the standard deviation of the length measurements between three frame points within each nine-frame average.

Height (km)	Velocity (km/s)	Error (km/s)
77.3	18.7	0.9
75.6	18.4	1.0
74.2	20.2	0.8
72.7	18.5	0.5
71.1	20.2	0.2
69.5	20.5	0.3
68.1	19.0	0.8
66.8	20.5	1.1
64.8	20.8	1.1
63.0	20.2	1.4
61.8	18.6	1.1

asteroid belt, we may estimate the probable source region for Park Forest. From Bottke et al. (2001) and taking a, e, i =2.53 0.68, 3.2° we find origin probabilities of 25% for the outer belt and Mars crossing population, 42% for the 3:1 mean-motion resonance, and 8% for the ν_6 secular resonance. The semi-major axis value for Park Forest is the largest of the eight known-meteorite orbits and, as noted by Morbidelli and Gladman (1998), leads to a strong dynamical selection toward origin at the 3:1 mean-motion resonance. Such large semi-major axis orbits also evolve quickly, so the residence time for

Table 2. Basic atmospheric trajectory data for the Park Forest fireball.

Time of maximum brightness	05:50:26.400 UT, March 27, 2003
Begin height (km)	82
End height (km)	<18
Begin latitude/long	41.13°N, 87.90°W
End latitude/long	41.46°N, 87.73°W
Maximum brightness (M_{vis})	−21.7
Radiant zenith angle	29.0°
Radiant azimuth	201°

Table 3. Heliocentric orbit for Park Forest.

α_r	$173.9 \pm 1.2°$
δ_r	$14.0 \pm 0.4°$
V_∞	19.5 ± 0.3 km/s
V_G	16.1 ± 0.4 km/s
α_G	$171.8 \pm 1.3°$
δ_G	$11.2 \pm 0.5°$
a	2.53 ± 0.19 AU
e	0.680 ± 0.023
i	$3.2 \pm 0.3°$
ω	$237.5 \pm 1.6°$
Ω	$6.1156 \pm 0.0007°$
q	0.811 ± 0.008 AU
Q	4.26 ± 0.38 AU

the Park Forest meteoroid after its escape from the main belt is likely to be have been only a few Ma (though its cosmic ray exposure age may be much longer given the various forces operating to diffuse material in the main belt [cf. Vokrouhlicky and Farinella 2000]).

INFRASONIC AND SEISMIC RECORDS OF THE FIREBALL AIRWAVE

The Park Forest fireball was detected infrasonically at the IS10 infrasound station near Lac Du Bonnet, Manitoba (range 1170 km) and at Blossom Point, Maryland (range 965 km). Infrasound is the portion of the atmospheric acoustic wave spectrum below ~20 Hz (sub-audible) and above the natural oscillation frequency of the atmosphere ($>~3 \times 10^{-3}$ Hz). Any mechanism that generates very large pressure gradients (sonic booms, thunderstorms, etc.) can produce infrasonic waves as well as higher frequency acoustic signals. The attenuation of infrasonic waves in the lower atmosphere is extremely low; typical signal amplitude losses are <<0.1 dB/km for f <10 Hz at ground level as compared to >10 db/km for f >50 Hz (cf. Gossard and Hooke 1975). It is this low attenuation and long range propagation which make infrasonic airwave measurements of interest.

Fig. 5 shows the airwave signals as seen at IS10 and Blossom Point. We are confident that, in both cases, this signal is associated with the fireball as the mean signal speed for both arrivals is consistent with stratospherically ducted signals (0.29 and 0.32 km/s, respectively; see Ceplecha et al. [1998] for details); the IS10 arrival shows a beam-formed azimuth (cf. Brown et al. 2002b for details of this procedure) within four degrees of the expected azimuth based on the fireball endpoint location and the signal duration (7–9 min) at both stations is very comparable to that observed for other fireball events at similar ranges. The Blossom Point station had only three of its four microphones in operation on the day of the event, so unique beamforming to measure the arrival azimuth of the signal is not possible from Fig. 5. The multiple maxima in the signal amplitude, however, are similar to the proximal seismic/acoustic recordings (see later) and consistent with the established multiple point-source detonations along the trajectory from the video/satellite data.

Previous work has provided relatively robust source energy estimates for a particular fireball based solely on measured infrasonic signals (cf. Brown et al. [2002b]; Borovička et al. [2003]; ReVelle et al. [2004]). Either (or both) of the period and peak amplitude of the infrasonic signal are used in these estimates, together with the theoretical approach described in ReVelle (1976). However, as noted in ReVelle (1976) the presence of winds may alter upwind or downwind characteristics of the signal, particularly the amplitude, but also signal periods in more extreme cases. The atmospheric conditions at the time of these earlier fireballs were (fortunately) relatively neutral with neither strong tropospheric or stratospheric winds to complicate analyses. Atmospheric winds at the time of the Park Forest fall are shown in Fig. 6. Values above 32 km are taken from the HWM model (Hedin et al. 1996), while those below 32 km were obtained from regional radiosonde measurements. It is immediately apparent that there is a strong tropospheric jet stream wind from the WNW at the time of the fall, with wind speeds near 40 m/s and a predicted stratospheric jet with comparable wind speeds near the altitude of 60 km.

While the observed signal periods at maximum amplitude are substantially different at IS10 and Blossom Point (5 and 2.3 sec, respectively), the ranges are similar to both stations from the fireball endpoint and wind conditions are almost exactly upwind and downwind, respectively. We make use of the period average as the best true estimate for the period at maximum amplitude of the source in wind-free conditions. Using this value for the period and the period at maximum signal amplitude-yield relationship given in ReVelle (1997), we find a source energy of 0.4 kt TNT equivalent from the infrasonic measurements.

Seismic recordings of the coupled airwave were detected at station BLO (39.1719°N, 86.5222°W) as shown in Fig. 7. At least five distinct arrivals are visible between 06:04:30 UT and 06:16 UT. Using the trajectory determined in the previous sections and modeling the airwave emission along the fireball path, we have been able to associate the first four of these arrivals with acoustic emission from two distinct points along the fireball path. This modeling used the INFRAMAP
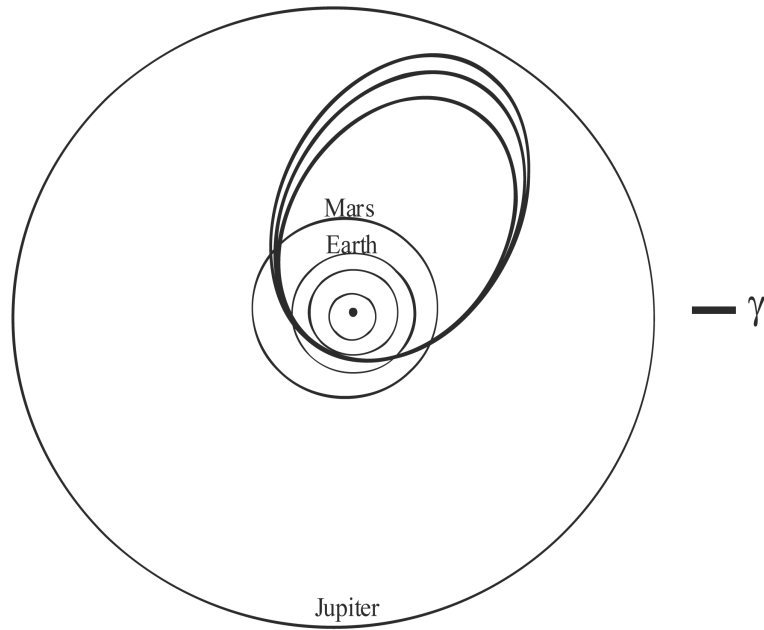
Fig. 4. Orbit for the Park Forest meteoroid. The central ellipse is the best estimated orbit and the outer and inner orbits represent the range of allowable sizes based on errors in the measurements (principally the velocity uncertainty). Also shown is the direction of the vernal equinox (γ).
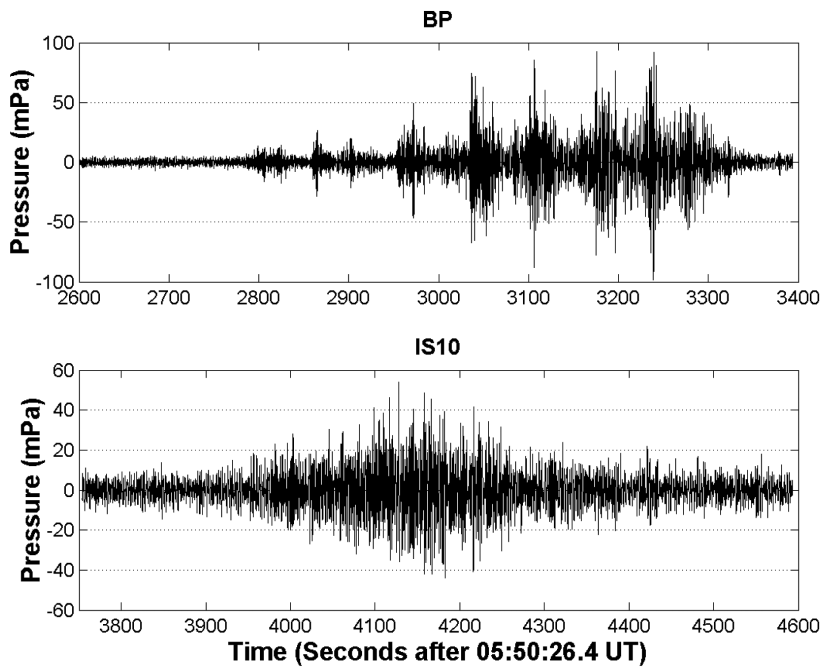

Fig. 5. Airwave signals from the Park Forest fireball as detected at IS10 (Lac Du Bonnet, Manitoba, (50°12′N, 96°1′W) and at Blossom Point, Maryland (38°25′N, 77°7′W). Only one channel is shown for each array. The signals have been bandpassed between 0.4–3 Hz for IS10 and 0.5–12 Hz for Blossom Point.

acoustic propagation code (Brown et al. 2002b). Results of the comparison of the modeling and observed airwave arrivals are shown in Table 4.

As is evident from the data (Table 4), these returns represent stratospheric and thermospheric paths from point sources located at the altitude of 17 km and 42 km. The amplitudes of the thermospheric arrivals are smaller than the stratospheric return as expected due to the larger attenuation present in the thermosphere for infrasonic signals (cf. Gossard and Hooke 1975). The first of these returns may correspond to the B4 flare from the video/satellite data, while the latter higher altitude source might be linked to the B0, the earliest
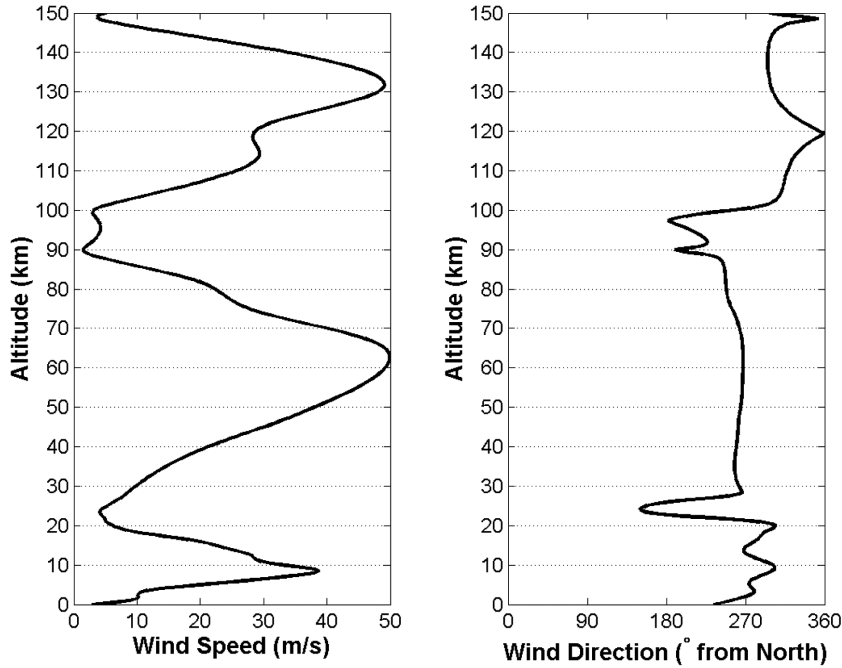
Fig. 6. Wind profiles at the time of the Park Forest fireball. The left panel shows the wind speed as a function of altitude and the right panel the wind direction. North is 0 azimuth in the right-hand plot. Note that the wind field below 32 km altitude is based on radiosonde data taken from Lincoln, Illinois at 0 UT on March 27, 2003. Wind values above 32 km are derived from the HWM model (Hedin et al. [1996]).
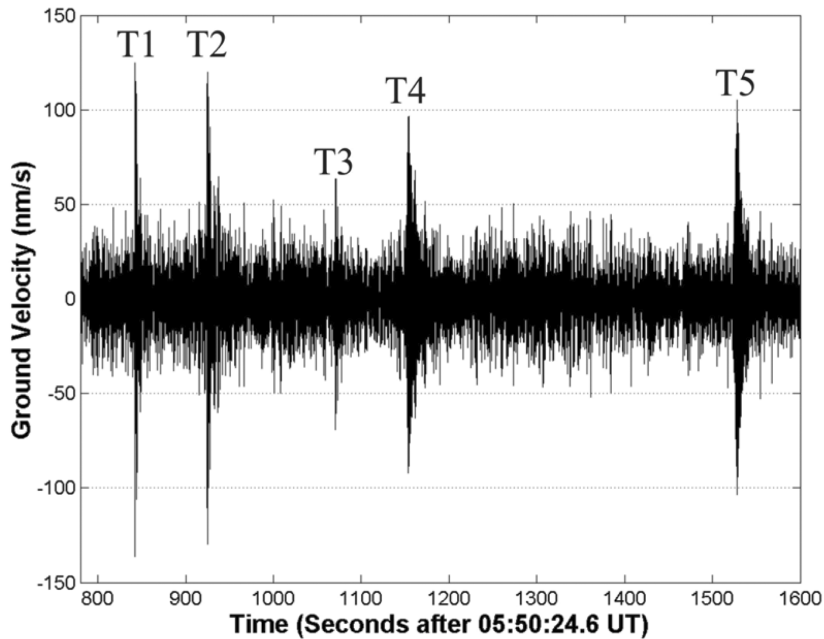

Fig. 7. Seismic airwave observed at seismic station Bloomington (39.1719°N, 86.5222°W). The apparent ground-velocity (with instrument response removed) is shown as a function of time relative to March 27, 2003 05:50:26.4 UT. Each of the arrivals listed in Table 4 are labelled.

fragmentation, though this is less certain. The lack of signal from the altitude regimes of the main burst may be explained partially by acoustic shadow zones notable below 40 km for the fireball-BLO geometry in the numerical ray-tracing results.

From the stratospheric returns, we may estimate crudely the total energy following the procedure outlined in Brown et al. (2002b). This estimate makes use of the observed peak velocity of the vertical component of the Rayleigh wave–airwave arrival corrected for range and scaled according to

Table 4. Properties of seismic signal arrivals and associated modeling results. The arrival notations are as shown in Fig. 7. Arrival times are in UT on March 27, 2003. The origin height is the point along the fireball trajectory where acoustic emission is determined to most closely match the observed delay time from modeling. The signal type indicates whether the best-match modeled waveform is stratospherically or thermospherically ducted, while Dev is the angular deviation in degrees away from the perpendicular for rays launched from the best-fit altitude. The delay time has been corrected for the finite fireball velocity and is referenced to the main burst at the altitude of 29 km.

Arrival	Arrival times	Delay (sec)	Origin height (km)	Signal type	Dev (degrees)	Ground range (km)	Seismic amplitude (nm/s)
T1	6:04:28	842	42	Strato	28.6	264	92
T2	6:05:50	924	17	Strato	17	278	105
T3	6:08:16	1070	42	Thermo	55	266	
T4	6:09:39	1153	17	Thermo	62	277	
T5	6:15:52	1526	–	–	–	–	

the local soil conditions. Specifically, we have that:

$$W = \frac{\chi R^2 (9.748 \times 10^{-11} D_v)^{1.738}}{\gamma} \qquad (2)$$

where D_v is the average vertical ground motion in nm/sec (zero-to-peak) over the three largest cycles of the Rayleigh wave train (corrected for the response of the seismometer), R is the range to the source in meters, W is the yield in kilotonnes of TNT equivalent energy, χ is the ratio of the air-to-ground coupling efficiency ratio for a surface explosion/airburst at altitude, and γ is the attenuation factor of the Rayleigh wave amplitude linked to the composition of the local ground relative to loose soil. We adopt the values of χ and γ from Brown et al. (2002b), which produced seismic energy estimates in reasonable agreement with the total energy of the Tagish Lake fireball found through other more precise methods. We find a total energy of 0.85 ± 0.15 kt TNT equivalent for the event in this way. We note that this formalism does not take into account the higher explosive altitude of the fireball burst as compared to the near-surface ground explosions used to define the original relation: the net effect should be to underestimate the total yield of the event.

In addition to these acoustic data, a security camera in Momence, Illinois recorded the audible detonations associated with the fireball approximately 2.5 minutes after the optical registration of the event. This station was less than 40 km total range from the terminal point and main detonation point observed by the satellite sensors; the raw (unprocessed) amplitude record from this camera is shown in Fig. 8. Applying the same modeling process as performed above for the seismic data as well as checking these results against the SUPRACENTER program (Edwards and Hildebrand 2003), it was possible to find the minimum time residual as a function of source height along the trajectory to associate with the three major arrivals. Both INFRAMAP and SUPRACENTER produced the same values within error. The first arrival is poorly constrained by the modeling—we can say only that the source height is near the altitude of 10 km and that it likely corresponds to the terminal supersonic flight/

fragmentation of some of the larger fragments. We suggest that the signal from the first arrival to the second arrival represents the terminal supersonic shock passage associated with the lower 5–10 km of the trail (the altitude of 12–22 km). The second arrival has minimal residuals for a height of 26.2 km and is associated with sound from the main burst (observed by the satellites to have occurred at the altitude of 29 km—MB in Fig. 3). The last arrival with a minimal residual at 35.3 km is almost certainly associated with the first early burst (B1 in Fig. 3) which satellite data places at 37 km. The systematic 1–2 km height difference between the acoustic results and satellite data may suggest either a small error in the atmospheric profile (overestimating the effective sound speed) or perhaps an error in the satellite heights. Other structure visible in the audio record may or may not be physically significant given the effects of automatic gain control feedback in the camera. We note that the acoustic rays from all of these point sources deviated by 20–40 degrees at the source from the perpendicular to the flight path, strongly suggesting their association with fragmentation events and not the main ballistic wave.

ABLATION MODELS

Gross Fragmentation Model

To better estimate the initial mass for Park Forest, we use the simple entry model employed to interpret the light curve and initial mass for the St-Robert and Tagish Lake fireballs (Brown et al. 1996; Brown et al. 2002b), namely that of the gross fragmentation model of Ceplecha et al. (1993). We make use of the known trajectory, as our starting conditions in this model and impose the constraints that our model output should reproduce closely the observed satellite light curve, the measured velocities along the trajectory and the mass of the largest fragment recovered on the ground. The total mass on the ground is difficult to measure precisely; a total of 18 kg has been documented, though it is probable that at least 30 kg has been recovered (Simon et al. 2004). A more realistic estimate accounting for the poor recovery conditions in parts
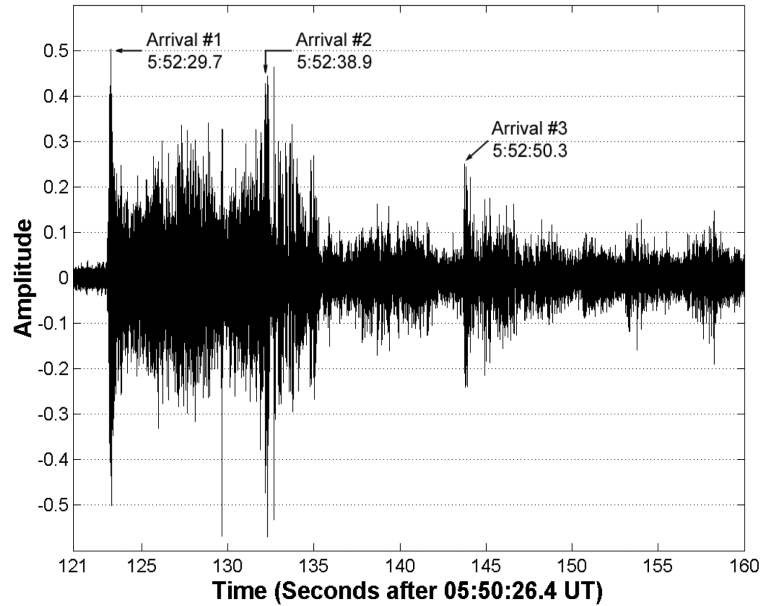
Fig. 8. Acoustic signal from the Park Forest fireball recorded by a security camera located in Momence, Illinois at a range of 40 km from the terminal detonation point of the fireball. The ordinate is the equivalent voltage recorded by the microphone, uncorrected for autogain control effects.
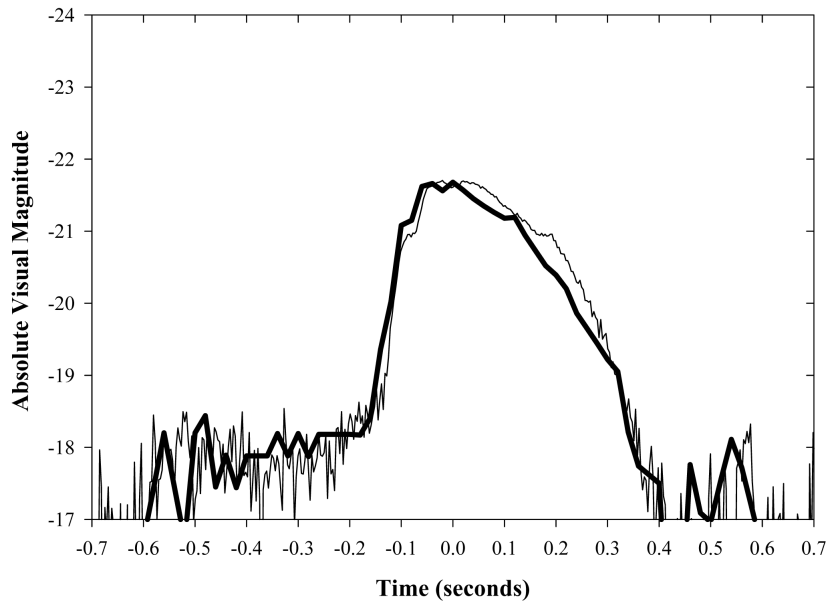

Fig. 9. Fireball light curve for Park Forest as recorded by space-based sensors of the U.S. DoE. The thin black line is the observed equivalent brightness in units of stellar magnitudes assuming 6000 K black body emission and using the conversion values given in Ceplecha et al. (1998). The thick black curve is the model fit from the gross fragmentation modeling of the event. The time in seconds is relative to March 27, 2003 05:50:26.4 UT.

of the ellipse might be at least several times this value. We may also estimate crudely the total ground mass by noting that the largest recovered fragments were 5.26 kg and 2.36 kg, respectively (Simon et al. 2004), and assume that the fragmentation size distribution follows that found for the Mbale meteorite shower (Jenniskens et al. 1994). Using this

approach, we estimate a minimum total mass on the ground near 45 kg, though this number is highly dependent on any unreported multi-kilogram-sized fragments.

To provide a baseline estimate for the ablation coefficient σ for modeling, we note that the Morávka meteorite fall (Borovička and Kalenda 2003) was best described with a

mean σ = 0.003 s^{2}km^{-2}; we use it as our starting value. We also assume a shape-density coefficient K (with $K = \Gamma A m^{-0.66}$, where Γ is the assumed drag coefficient, A is the cross sectional area, and m is the mass) of 0.46 (Ceplecha et al. 1998) as appropriate for chondritic bodies. The model fit to the light curve is shown in Fig. 9. We note that the velocity fit is good for the early portion of the trajectory, but generally above the 14 km/s mean found from satellite data in the last stages of the event (from the altitude of 28–22 km as shown in Table 1), the model velocity being 16 km/s at the altitude of 22 km. As the model implicitly follows a single body (and light is produced as soon as material ablates from this body), the most likely explanation is that the object was not a single monolithic stone with a small cloud of fragments in the latter portion of the trajectory, but more likely a collection of many large fragments. Such behavior has been clearly documented by Borovička and Kalenda (2003) associated with the Morávka meteorite fall. The single body nature of the gross fragmentation model clearly fails to reproduce dynamics in such circumstances, though we expect the initial total mass to be reflected accurately in the total integrated light produced in flight. Our observational data are simply too coarse to place meaningful constraints on the actual dynamics at the end of the trail; we can constrain only the total mass via the observed light production.

From the model, we find that the dynamic pressure experienced by Park Forest at the time of its first major fragmentation (37 km altitude) was 2.4 MPa, while the pressure at the major burst point at 29 km altitude was 7 MPa. This places Park Forest near the peak in the typical fragmentation dynamic pressure observed for bright fireballs (Ceplecha 1993). These fragmentation pressures are also similar to those found by Borovička and Kalenda (2003) for the Morávka fireball where individual fragmentation events had ram pressures between 2–5 MPa. Our estimate of the pressure at 29 km may be too high by 20–30% if the deceleration observed by the satellite systems at lower altitudes is more accurate as discussed earlier. We also find evidence in the SHPD video for very early fragmentation (in the form of elongation of the fireball head and production of a debris trail) near the altitude of 70 km under ram pressures of 0.8 MPa. The elongated trail is visible for 2.4 km behind the main body. Such early fragmentation behavior is a common feature of larger fireballs as noted by Borovička and Kalenda (2003) and suggests the presence of cracks or fissures in the main body. Our final model fit yields an estimate of the initial mass of 14 tonnes the equivalent to a meteoroid ~2 m in diameter.

Porosity Model

We have also modeled this event using techniques developed recently to fully characterize bolide entries (cf. ReVelle 2001; ReVelle 2002). This model is a compendium of numerous separate approaches to a large body meteoroid ablation developed earlier (ReVelle 1979) and which have been modified explicitly to include meteoroid porosity. Most recently, this model was successfully applied to the Tagish Lake meteorite fall (Brown et al. 2002b). We start by using the approximate initial mass for Park Forest found from the gross fragmentation model (radius of initial body = 1 m) and check the consistency of the light production, dynamics, and final mass using this more refined model. All entry parameters are taken from Tables 1 and 2.

We have applied this set of conditions to the fall of the Park Forest meteorite by varying the porosity of the body, assuming that no fragmentation occurs until the ram pressure equals a preset value (taken from the literature, see ReVelle [2002] for details) and taking the estimated bulk density of the Park Forest (L5) meteorites to be 3400 kg/m^3 (Consolmagno and Britt 1998). Presently, it is assumed that a maximum of 100 fragments are produced and a geometric progression with time of the pieces occurs as fragmentation begins. It is also assumed that all fragments are of the same size in both the dynamics and in their contribution to the light curve. The porosity value is changed until the best possible fit to the dynamics, end mass, and light curve result.

The nominal panchromatic passband is from 360–675 nm, whereas the nominal optical satellite passband is from 400–1200 nm. As such, we do not expect perfect agreement between the current modeling prediction and satellite observations. The peak magnitude and the declining portions of the light curve are matched well to the observed values from satellite data though the model predicts higher luminosities in the early portion of the flight than is observed. Our best fit initial body value is a radius of 0.90 m with 40% internal porosity representing an initial mass of ~7×10^3 kg. These initial values reproduce the observed velocity profile well, penetrate to the correct end height (near 18 km), and produce final mass on the ground of 150 kg. The discrepancy in the light curve at higher altitudes cannot be rectified by simply changing the potential porosities (as the dynamics/end mass/end heights will not match in that case). We believe that the primary cause of this discrepancy is the assumed nature of the fragmentation process in the model—it may be necessary to take this as a free parameter to more fully match the light curve and produce a better estimate of the initial mass.

We also present the expected power balance for the respective differential efficiencies of heat, panchromatic light, acoustic, dissociation, ionization, and of the total process in Fig. 10 based on the porosity modeling. Differential efficiencies were calculated along the Park Forest trajectory with all of the values linked directly to the semi-empirical panchromatic luminous efficiency with the exception of the differential acoustic efficiency. The acoustic efficiency was calculated directly from first principles by computing the kinetic energy density of the blast wave at x = 1 (one blast wave radius away from the trajectory) (cf.
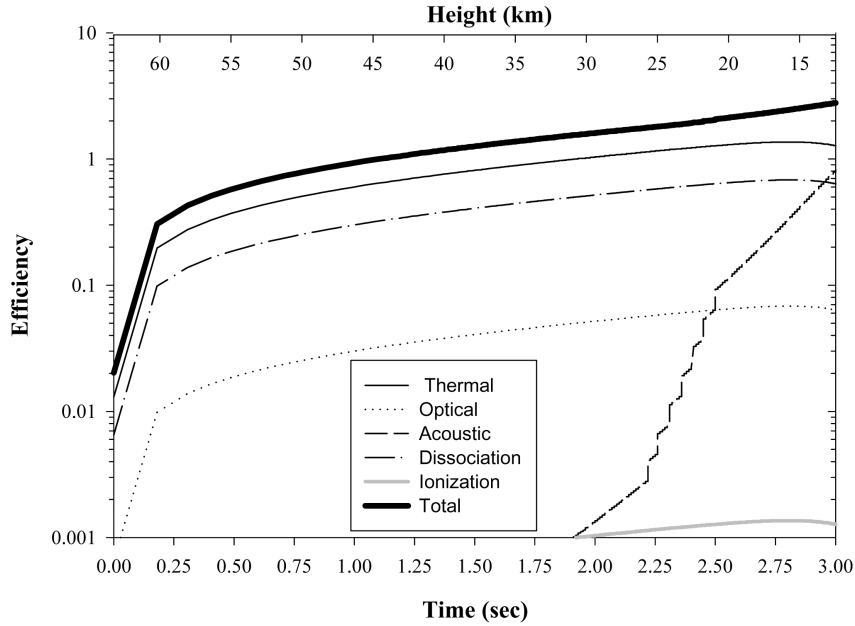
Fig. 10. Predicted differential efficiencies of heat, panchromatic light, acoustic, dissociation, ionization, and of the "total" power balance versus time (sec).

ReVelle 1976 for details) compared to the total kinetic energy deposited at that point on the trail per unit volume. Its increase with time at the latter stages of the flight result from continued fragmentations that have been triggered once the stagnation pressure on the front face exceeded the breaking strength, and the assumption that the fragments deposited into the wake remain there throughout the flight as they continue ablating and producing light. The other efficiencies were all calculated as ratios with respect to the luminous efficiency employing historical laboratory data using simple functional relationships. Although still in need of improvement, the vast majority of the kinetic energy change with time of the bolide has been accounted for, the primary exception at the very earliest stages of the entry where it is expected to be very small. More details can be found in ReVelle (2001) and ReVelle (2002).

Dark Flight

In an effort to link the broad characteristics of the observed meteorite strewn-field pattern with the atmospheric dynamics of the fireball, the predicted location of fragments on the ground based on dark flight modeling was computed. This process is described in detail in Brown et al. (1996) and Borovička and Kalenda (2003). Basically, the procedure involves using the output of the theoretical gross fragmentation model and the probable location along the trajectory where fragments decelerate below the speed at which ablation takes place. Typically this speed is 3–4 km/s based on the terminal velocity observed for many bright fireballs (cf. Ceplecha et al. 1998). Once the initial "ejection"

point along the trajectory and velocity vector is defined, the dark flight modeling follows fragments of different masses under the influence of upper winds to the ground. Normally this "ejection" point would be taken to be the last luminous portion of the fireball path. In our case, the lowest point for which substantial ablation has been recorded is from the IR satellite data at an altitude of 18 km. Our gross fragmentation modeling suggests the largest fragment would reach 4 km/s near the altitude of 15 km. We have bracketed our launch altitudes for 22, 29, and 37 km to correspond with the major burst heights established from the video/satellite data and the lowest altitude. In an effort to explore how wide variations in the assumed initial conditions change the fall distribution we have chosen two starting models. In the first model, we begin dark flight at the burst points, i.e., all fragments are forced to 4 km/s at the height of burst and then followed to the ground without further ablation, a highly artificial assumption. However, if our theoretical model is overestimating the velocity at lower heights along the trajectory as a result of widespread hierarchical fragmentation of the meteoroid (as suggested earlier in the gross fragmentation model section) then we might expect this model to more closely reproduce the ground distribution. In our second and more physically realistic model (within the context of a single meteoroid body assumption), we take fragments from release at each burst height and continue following their mass loss and deceleration until they reach 4 km/s. At this point we assume that ablation ceases and we begin following further flight of the fragment under dark flight conditions.

Fig. 11 shows both the observed distribution on the ground (adapted from Simon et al. 2004) and that predicted
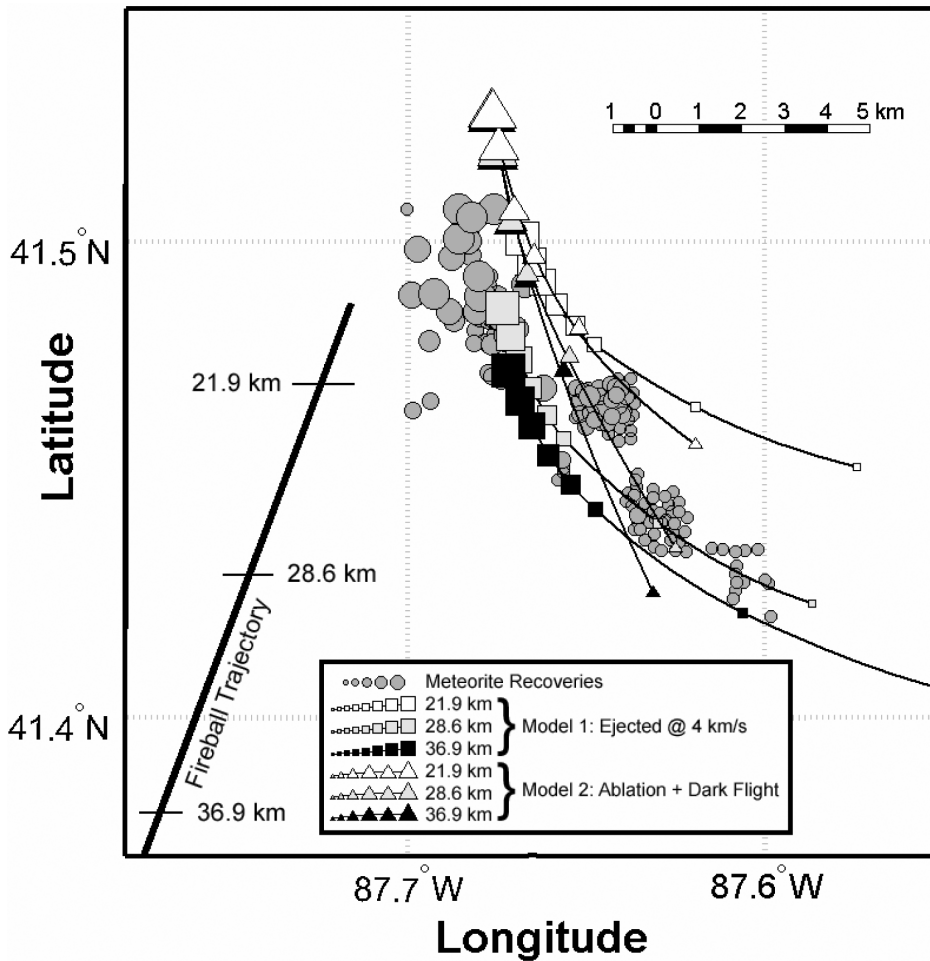
Fig. 11. An estimate of fragment locations on the ground following results of dark flight modeling. The filled circles represent recovered fragments of varying masses (see Simon et al. 2004), while the solid squares show the estimated fall locations for fragments of differing masses released at 4 km/s (model 1) at different burst altitudes (see legend). The masses modeled were 5.26 kg, 2.67 kg, 1.5 kg, 0.75 kg, 0.375 kg, 0.2 kg, 0.02 kg and 0.002kg with the symbols going from the largest to the smallest as mass decreases. The triangles represent fragments followed from each of the three burst heights with starting velocities equal to the same velocity as the main body and continuing ablation until a velocity of 4 km/s is reached (model 2). The masses modeled were 5.7 kg, 2.67 kg, 0.7 kg, 0.3 kg, 0.05 kg and 0.003 kg.

by dark flight modeling. The most obvious characteristic from both models is the large rotation of the fall ellipse toward the south-east, a direct consequence of the strong tropospheric jet stream winds from the west. All fragments ejected at the three main detonation points from each model along the trajectory are shown. Fragments released directly into dark flight at the burst points (model #1) overlap the strewn-field well and suggest that fragments of various masses may have come from across the entire height range from 38 to 22 km and that our modeled velocities in the lower portion of the trail are too high. Those followed from the burst point through further ablation (model #2) are substantially further removed (to the north and east) from the observed fall, indicating perhaps that larger fragments were "released" higher along the trajectory, and decelerated to sub-luminous velocities well before 15 km altitude. There is a systematic shift in the magnitude of the apparent mass to the SE; i.e., modeled masses (particularly at

the largest masses) are systematically too high for the portion of the strewn-field closest to individual landing points. A similar effect was noted by Borovička and Kalenda (2003) in connection with the Morávka meteorite fall.

Possible reasons for this effect include an error in the magnitude/direction (or height intervals) of the tropospheric jet or perhaps cross-wind flight associated with non-zero lift coefficients (which our dark flight model assumes are all zero). While the latter cannot be ruled out, the relatively large spatial gradients associated with tropospheric jets and the fact that our upper air data are taken over 200 km from the fall location lead us to favor the former explanation.

DISCUSSION AND CONCLUSIONS

A summary of the estimated energies/masses and sizes for the initial Park Forest meteoroid is given in Table 5. The

Table 5. Summary of mass and energy estimates for the Park Forest meteoroid. Mass estimates are made assuming an initial entry velocity of 19.5 ± 0.3 km/s, while radius measurements assume an average bulk density of 3400 kgm^{-3} as appropriate for L5 chondrites (Consolmagno and Britt 1998).

Technique	Energy estimate (kt TNT)	Mass estimate (kg)	Equivalent radius (m)
Satellite empirical τ	0.41 ± 0.09	$(8.58 \pm 1.88) \pm 10^3$	0.845 ± 0.185
Gross fragmentation model	0.64 ± 0.02	1.4×10^4	0.99
Infrasound	~0.4	8.5×10^3	0.84
Seismic	$\approx 0.85 \pm 0.15$	$(1.8 \pm 0.3) \times 10^4$	1.12 ± 0.19
Porosity model	~0.3	$\sim 7 \times 10^3$	0.90

range of acceptable masses based on all techniques is ~7000–20000 kg, though results from the most robust methods lead us to conclude the most probable value is likely $(11 \pm 3) \times 10^3$ kg. The measurement of the initial velocity with relatively good precision has been possible by combining ground-based video data having high temporal resolution with satellite determination of the trajectory to yield an initial velocity estimate of 19.5 ± 0.3 km/s.

This relatively high initial velocity may help explain why relatively little mass has been recovered on the ground (despite good conditions in the fall area) as survival of meteoritic material strongly depends on velocity (Ceplecha et al. 1998). Formal estimates of the likely mass on the ground range from 18 kg, representing reported finds, to more than ~50 kg based on an assumed fragmentation distribution. These estimates suggest that 0.1%–0.5% of the initial meteoroid survived as ponderable fragments reaching the ground.

The zenith angle of the fireball radiant has been determined from satellite data to be 29°, while the fireball detected by the satellite sensors down to an altitude below 18 km first appears at a height of 82 km based on video recordings. Some indication of supersonic flight by some fragments for several additional kilometers below this altitude is suggested by modeling results associated with the nearby microphone recording of the fireball acoustic signal. The peak absolute visual brightness of the fireball was near −22, a magnitude reached at the height of 28 km. Three major detonations were recorded by both satellite sensors and all the studied ground-based video recordings at the altitudes of 37, 29, and 22 km. There are additional indications of lesser flares near an altitude of 41 km and 19 km from video data.

There are clear hints of early, minor fragmentation in the video record near 70 km altitude under less than one MPa of ram pressure. All major fragmentations occurred with pressures of 2–7 MPa in the later stages of flight. These values are comparable to those found for other fireballs believed to be of stony composition (Ceplecha 1993) and associated with other meteorite-dropping fireballs (Borovička et al. 2003). These results suggest that the true global "binding" strength for meter-sized NEAs of stony composition may be two orders of magnitude lower than their compressive strengths and one order of magnitude lower than their tensile strengths as compared to these same values measured for ordinary chondrites in the laboratory

(Medvedev 1985). This conclusion is further supported by the inferred rotation periods for meteoroids measured from fireball data which suggest limiting rotational rates consistent with strengths of 1–10 MPa for objects down to diameters of ~0.1 m (Beech and Brown 2000). This result suggests that even very small NEAs may not be true monolithic stony bodies but rather bound aggregates (or quasi-rubble piles), the ultimate strengths of which are determined perhaps by shock fractures or other imperfections. If this strength measure derived specifically from Park Forest (and more generally supported by other fireball data) is an accurate representation of the equivalent tensile strength for small NEAs, it implies further that small NEAs will have limiting rotational periods much higher than would be expected assuming true "monolithic" bodies as suggested on theoretical grounds by others (Holsapple 2004). Fig. 12 shows the equivalent limits computed assuming the required centripetal force per unit area just matches the binding strength (shown for two values of 1 MPa and 5 MPa). Observations of small, fast rotating NEAs are now approaching the period limits suggested here (as shown in the figure) and as the observational statistics for this population increase, we predict limiting periods near 20–30 sec for small rotators (<100 m in radius) will be observed.

The heliocentric orbit for Park Forest is relatively normal, being a typical Apollo-type asteroid, low inclination orbit with perihelia well inside Earth's orbit. The semi-major axis and aphelion distance are the largest of the eight measured meteorite orbits, though the orbit still lies well inside Jupiter's orbit. Using the source-region model for NEAs of Bottke et al. (2001), we find that Park Forest has a 25% probability of originating in either the outer belt or the Mars-crossing population, a 42% probability of being released from the 3:1 mean-motion resonance and an 8% probability of association with the 6 secular resonance.

The acoustic signals produced by the Park Forest fireball were dominated by fragmentation events. The stratospheric signals were produced by acoustic radiation with deviations of <30 degrees from the perpendicular to the trajectory, consistent with estimates of fragmentation radiation directions made for the Morávka meteorite fall. Neither the seismic nor the security camera audio recording showed a clear ballistic wave arrival, perhaps a result of the geometry of the trail relative to these stations.
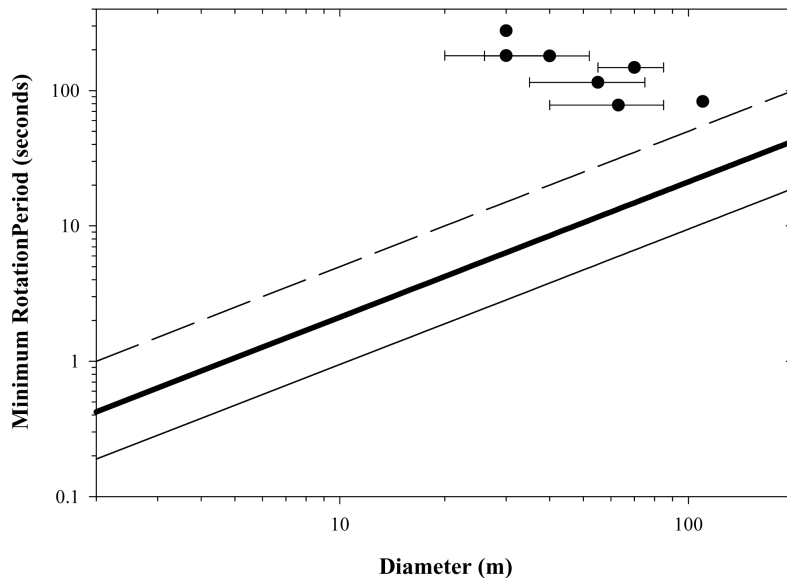
Fig. 12. The limiting rotational period for small near-Earth asteroids as a function of their diameter for two limiting tensile strengths based on observed breaking pressures for the Park Forest meteoroid. The thick line is for 1 MPa and the thin line for 5 MPa tensile strength limits. The dashed line is the limit derived from inferred fireball rotational measurements by Beech and Brown (2000). Solid circles represent observed asteroid rotational periods from Binzel et al. (2002) and recent compilations from Pravec (http://www.asu.cas.cz/~ppravec/newres.htm).

Editorial Handling—Dr. Michael Gaffey

REFERENCES

Beech M. and Brown P. 2000. Fireball flickering: The case for indirect measurement of meteoroid rotation rates. *Planetary and Space Science* 48:925–932.

Binzel R. P., Lupishko D., Di Martino M., Whitely R., and Hahn G. J. 2002. *Physical properties of near-Earth object in asteroids III,* edited by Bottke W. F., Cellino A., Paolicchi P., and Binzel R. P. Tucson: University of Arizona Press. pp. 255–271.

Borovička J. and Kalenda P. 2003. The Morávka meteorite fall: 4. Meteoroid dynamics and fragmentation in the atmosphere. *Meteoritics & Planetary Science* 38:1023–1045.

Borovička J., Spurný P., Kalenda P., and Tagliaferri E. 2003. The Morávka meteorite fall: 1. Description of the events and determination of the fireball trajectory and orbit from video records. *Meteoritics & Planetary Science* 38:975–989.

Bottke W., Morbidelli A., Jedicke R., Petit J-M., Levison H., Michel, P, and Metcalfe T. 2001. Debiased orbital and size distributions of the near-Earth objects. *Icarus* 156:399–433.

Bland P. and Artmemieva N. A. 2003. Efficient disruption of small asteroids by Earth's atmosphere. *Nature* 424:288–291.

Brown P., Hildebrand A. R., Green D. W. E., Page D., Jacobs C., ReVelle D., Tagliaferri E., Wacker J., and Wetmiller B. 1996. The fall of the St-Robert meteorite. *Meteoritics & Planetary Science* 31:502–517.

Brown P. G., Hildebrand A. R., Zolensky M. E., Grady M., Clayton R. N., Mayeda T. K., Tagliaferri E., Spalding R., Macrae N. D., Hoffman E. L., Mittlefehldt D. W., Wacker J. F., Bird J. A., Campbell M. D., Carpenter R., Gingerich H., Glatiotis M., Greiner E., Mazur M. J., Mccausland P. J. A., Plotkin H., and Rubak Mazur T. 2000. The fall, recovery, orbit, and composition of the Tagish Lake meteorite: A new type of carbonaceous chondrite. *Science* 290:320–325.

Brown P. R. E., Spalding D.O., ReVelle, E. Tagliaferri, and S. P. Worden. 2002a. The flux of small near-Earth objects colliding with the Earth. *Nature* 420:294–296.

Brown P., ReVelle D. O., Tagliaferri E., and Hildebrand A. R. 2002b. An entry model for the Tagish Lake fireball using seismic, satellite and infrasound records. *Meteoritics & Planetary Science* 37:661–676.

Ceplecha Z. 1987. Geometric, dynamic, orbital and photometric data on meteoroids from photographic fireball networks. *Bulletin of the Astronomical Institutes of Czechoslovakia* 38:222–234.

Ceplecha Z., Spurný P., Borovička J., and Keclíková J. 1993. Atmospheric fragmentation of meteoroids. *Astronomy and Astrophysics* 279:615–626.

Ceplecha Z., Borovička J., Elford W. G., ReVelle D. O., Hawkes R. L., Porubčan V., and Šimek M. 1998. Meteor phenomena and bodies. *Space Science Reviews* 84:327–471.

Consolmagno G. and Britt D. 1998. The density and porosity of meteorites from the Vatican collection. *Meteoritics & Planetary Science* 33:1231–1241.

Edwards W. N. and Hildebrand A. R. 2004. SUPRACENTER: Locating fireball terminal bursts in the atmosphere using seismic arrivals. *Meteoritics & Planetary Science* 39:1449–1460.

Gossard E. E. and Hooke W. H. 1975. *Waves in the atmosphere: Atmospheric infrasound and gravity waves—their generation and propagation*. Amsterdam: Elsevier Press. 470 pp.

Hedin A. E., Fleming E. L., Manson A. H., Schmidlin F. J., Avery S. K., Clark R. R., Franke S. J., Fraser G. J, Tsuda T., Vial F., and Vincent R. A. 1996. Empirical wind model for the upper, middle, and lower atmosphere. *Journal of Atmospheric and Terrestrial Physics* 58:1421–1447.

Holsapple K. A. 2004. Could fast rotator asteroids be rubble piles? (abstract #1792) 34th Lunar and Planetary Science Conference. CD-ROM.

Hills J. G. and Goda M. P. 1993. The fragmentation of small asteroids in the atmosphere. *The Astronomical Journal* 105:1114–1144.

Jenniskens P., Betlem H., Betlem J., Barifaijo E., Schluter T., Hampton C., Laubenstein M., Kunz J., and Heusser G. 1994. The Mbale meteorite shower. *Meteoritics* 29:246–254.

McCord T. B., Morris J., Persing D., Tagliaferri E., Jacobs C., Spalding R., Grady L., and Schmidt R. 1995. Detection of a meteoroid entry into the Earth's atmosphere on February 1, 1994. *Journal of Geophysical Research* 100:3245–3249.

Medvedev R. B., Gorbatsevich F. F., and Zotkin, I. T. 1985. Determination of the physical properties of stony meteorites as applicable to a study of the processes of their breakup. *Meteoritika* 44:105–110.

Morbidelli A. and Gladman B. 1998. Orbital and temporal distributions of meteorites originating in the asteroid belt. *Meteoritics & Planetary Science* 33:999–1016.

National Imagery and Mapping Agency. 2000. *Department of Defense World Geodetic System 1984: Its definition and relationships with local geodetic systems*, 3rd edition. Bethesda, Maryland: NIMA.

ReVelle D. O. 1976. On meteor-generated infrasound. *Journal of Geophysical Research* 81:1217–1240.

ReVelle D. O. 1979. A quasi-simple ablation model for large meteorite entry: Theory versus observations. *Journal of Atmospheric and Terrestrial Physics*. 41:453–473.

ReVelle D. O. 1997. Historical detection of atmospheric impacts of large super-bolides using acoustic-gravity waves. *Annals of the New York Academy of Sciences*. 822:284–302.

ReVelle D. O. 2001. Bolide dynamics and luminosity modeling: Comparisons between uniform bulk density and porous meteoroid models. In *Proceedings of the Meteoroids 2001 Conference*, edited by Warmbein B. ESA SP-495. Noordwijk: European Space Research and Technology Research Center. pp. 513–518.

ReVelle D. O. 2002. Fireball dynamics, energetics, ablation, luminosity and fragmentation modeling. In *Proceedings of the Conference Asteroids, Comets, Meteors (ACM 2002)*, edited by Warmbein B. ESA SP-500. Noordwijk: European Space Research and Technology Research Center. pp. 127–136.

ReVelle D. O. and Ceplecha Z. 2002. Semi-empirical fragmentation model of meteoroid motion and radiation during atmospheric penetration. In *Proceedings of the Conference Asteroids, Comets, Meteors (ACM 2002)*, edited by B. Warmbein. ESA SP-500. Noordwijk: European Space Research and Technology Research Center. pp. 285–288.

ReVelle D. O., Brown P. G., and Spurný P. 2004. Entry dynamics and acoustics/infrasonic/seismic analysis for the Neuschwanstein meteorite fall. *Meteoritics & Planetary Science* 39:1605–1626.

Simon S. B., Grossman L., Clayton R. N., Mayeda T. K., Schwade J. R., Sipiera P. P., Wacker J. F., and Wadhwa M. 2004. The fall, recovery, and classification of the Park Forest meteorite. *Meteoritics & Planetary Science* 39:625–634.

Spunrý P., Oberst J., and Heinlein, D. 2003. Photographic observations of Neuschwanstein, a second meteorite from the orbit of the Príbram chondrite. *Nature* 423:151–153.

Tagliaferri E., Spalding R., Jacobs C., Worden S. P., and Erlich A. 1994. Detection of meteoroid impacts by optical sensors in Earth orbit. In *Hazards due to comets and asteroids*, edited by Gehrels T. Tucson: The University of Arizona Press. pp. 199–220.

Vokrouhlický D. and Farinella P. 2000. Efficient delivery of meteorites to the Earth from a wide range of asteroid parent bodies. *Nature* 407:606–608.